This is an *Accepted Manuscript*, which has been through the Royal Society of Chemistry peer review process and has been accepted for publication.

Accepted Manuscripts are published online shortly after acceptance, before technical editing, formatting and proof reading. Using this free service, authors can make their results available to the community, in citable form, before we publish the edited article. We will replace this *Accepted Manuscript* with the edited and formatted *Advance Article* as soon as it is available.

You can find more information about *Accepted Manuscripts* in the **Information for Authors**.

Please note that technical editing may introduce minor changes to the text and/or graphics, which may alter content. The journal's standard **Terms & Conditions** and the **Ethical guidelines** still apply. In no event shall the Royal Society of Chemistry be held responsible for any errors or omissions in this *Accepted Manuscript* or any consequences arising from the use of any information it contains.

Journal Name

ARTICLE TYPE

Facet-dependent catalytic activity of MnO electrocatalysts for oxygen reduction and oxygen evolution reactions

Chung-Hao Kuo,[a] Islam M. Mosa,[a] Srinivas Thanneeru,[a] Vinit Sharma,[b] Lichun Zhang,[b] Sourav Biswas,[a]
s **Mark Aindow,[b] S. Pamir Alpay,[b] James F. Rusling,[a] Steven L. Suib,[a,b],* Jie He[a],***

This Communication highlights the facet-dependent electrocatalytic activity of MnO nanocrystals for OERs/ORRs. The MnO
10 **(100) facets with higher adsorption energy of O species can largely promote the electrocatalytic activity.**

To meet the growing demands of renewable energy, various electrochemical energy conversion processes between O_2 and H_2O, *e.g.* oxygen evolution reaction (OER) and oxygen reduction reac-
15 tion (ORR) that are of great importance for solar water splitting and fuel cells, have received much attention in the past decade.[1] A key technical barrier to achieve highly efficient OERs and ORRs is the kinetically slow electron-transfer in which four electrons are involved.[2] The rational design of active electrocatalysts is central
20 to these energy conversion techniques. Traditionally, expensive Pt and its bimetallic alloys have traditionally been the most active catalysts for the ORR;[3] and precious metal oxide IrO_2 and RuO_2 catalysts have proved to be very efficient for the OER.[4] However, the large-scale commercialization of these catalysts is limited by, i)
25 the cost effectiveness of the requisite raw materials, and ii) considerable overpotential (η) required for both the OER and ORR (0.3~0.8 V). The earth-abundant and inexpensive transition metal oxides, *e.g.* manganese oxides (MnO_x), have been explored as alternative electrocatalysts for OERs and ORRs under alkaline con-
30 ditions.[5] MnO_x families have over 30 different crystal structures and variable valence of Mn centers in different polymorphs.[6] Despite numerous reports on the electrocatalytic performance of MnO_x for OERs and ORRs, insight into the effect of structural parameters, *e.g.* topological structures, surface compositions and
35 energy, and valance of Mn centers on their catalytic activity, is still lacking.[5]

In heterogeneous catalysts, control of complex anisotropic structures with preferentially exposed crystal planes or surface atoms is a key to achieving a high catalytic selectivity and activity.
40 Moreover, the surface interactions between O species and catalytic centers towards the formation of O-O bonds in -OOH species on catalytic centers, dominate the reaction activity of both the OER and the ORR. To this end, for MnO_x families, a fundamental understanding of correlations between the catalytic performance for
45 OER and ORR and surface properties is urgently needed. As a prototype system, we herein choose to concentrate on a simple halite MnO with a face-centered cubic (*fcc*) structure to evaluate the effect of surface energy on catalytic activity for both OER and ORR. 3-D complex MnO nanoflowers and polypods with selective-
50 ly oriented MnO crystals were prepared using a limited ligand protection method. Electrocatalytic measurements demonstrated

that the catalytic activity of MnO nanocatalysts for both OER and ORR was highly dependent on exposed crystal planes. Our study highlights the correlation between OER/ORR activities and ex-
55 posed crystal planes of manganosite catalysts and it may provide fundamental guidance for developing active and cost-effective electrocatalysts.
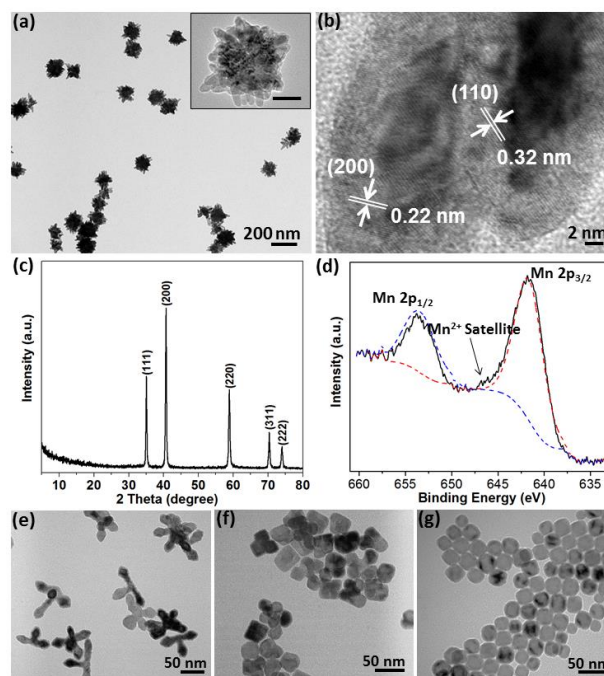
60 **Fig 1.** (a,b) TEM images of MnO nanoflowers. The inset in (a) is a zoom-in view of a single nanoflower. (c) The powder XRD pattern of MnO nanoflowers. (d) Mn 2p XPS spectrum of MnO nanoflowers. (e-g) TEM images of MnO nanocrystals obtained at different $Mn(oleate)_2$/OA molar ratios: (e) 1:0.09; (f) 1:0.27; (g) 1:0.9.

65

MnO nanoflowers and polypods were synthesized by using thermal decomposition of $Mn(oleate)_2$ in a non-coordinating, apolar hydrocarbon solvent.[7] Briefly, 1.24 g of $Mn(oleate)_2$ was dissolved in 10 g of octadecene in a 25 mL three-neck round-bottom
70 flask. The mixture was first degassed at 80°C under vacuum for 30 min and then heated to 320 °C at a rate of 10 °C/min under argon. After stirring for another 30 min, the reaction mixture was cooled and then precipitated with an excess of acetone. The obtained nanoparticles (NPs) were first characterized by transmission electron

microscopy (TEM). As shown in the low-magnification TEM image (Fig 1a and more images in Fig S1), the nanoflowers are composed of a spherical core decorated by densely packed well-defined MnO nanorods. The as-synthesized MnO nanoflowers are quasi-spherical and have an average diameter of 126.5 ± 17.6 nm (Fig S2). These nanorods are nearly single crystalline MnO (see below) and have a length of 40~50 nm and a diameter of ~15 nm. High-resolution TEM analysis showed the manganosite crystalline structure of MnO with d-spacings of 0.22 nm and 0.32 nm that correspond to (200) and (110) planes (Fig 1b), in good agreement with the powder X-ray diffraction (XRD) pattern in Fig 1c. The deconvolution of X-ray photoelectron spectroscopy (XPS) data (Fig 1d) shows the binding energy of Mn $2p_{1/2}$ (653.4 eV) and Mn $2p_{3/2}$ (641.6 eV) falls in the Mn 2p region.[5a] The co-existence of a satellite peak at 646 eV suggests the presence of Mn^{2+} species on the surface of the nanoflowers. X-ray absorption near-edge spectra also confirmed the average Mn oxidation state of 2.02 (Fig S8). No significant amount of Mn species with higher oxidation state was detected for months.

The oriented attachment of 1D nanorods to nanoflowers, *e.g.* the number and length of 1D nanorods, appeared to be highly controllable using oleic acid (OA) as a free ligand. These results are summarized in Figs 1e-g (see more TEM images in Figs S3-5). At a low concentration of OA (Mn(oleate)$_2$/OA=1:0.09, mol/mol, M/O ratio hereafter), the formation of MnO polypods was observed (Fig 1e). These polypods essentially retained the 3-D complex architectures of nanoflowers but had far fewer branches. Of them, MnO tetrapods composed of four nanorod branches were the dominant product. Compared to MnO nanoflowers, the length and diameter of nanorods in MnO polypods did not change significantly. With increase of M/O ratio to 1:0.27 (mol/mol), irregular polyhedra with surface protuberances were obtained where MnO nanorods were significantly shortened (Fig 1f). The average size of MnO polyhedra decreased to ~32 nm. By further increasing the M/O ratio to 1:0.9 (mol/mol), the complex surface structures disappeared and nearly mono-disperse MnO octahedral nanocrystals were obtained with a diameter of ~19 nm (Fig 1g).

The growth of MnO 3-D complex nanocrystals was likely due to the limited ligand supply.[7a] Without the presence of OA free ligands, the initially formed MnO seeds were not covered by OA ligands; thus, the growth of MnO nanocrystals was nucleated on the exposed surface of MnO seeds. Limited ligand protection would lead to the formation of nanoflowers with oriented nanorods. In the presence of a low concentration of OA ligands (<20 mol%), the OA would partially cover the surface of MnO seeds. The less exposed surface resulted in the formation of MnO polypods with much less branched nanostructures. With the addition of 1: 0.9 equivalence of OA ligands, the (111) planes of MnO seeds were preferentially bonded with OA ligands thus leading to the formation of octahedral MnO nanocrystals.

To gain more insight into the crystallographic structure and growth mechanism of MnO nanocrystals, high resolution TEM characterization with selected area electron diffraction (SAED) studies were further performed. The results of surface planes of MnO nanocrystals are intriguing. The TEM image of a single nanorod on MnO polypods (Fig 2a) shows the (200) and (110) planes with an interfacial angle of 45°. The SAED pattern of nanorods can be indexed to the manganosite *fcc* structure with the <100> zone axis parallel to (001) and (010) planes (Fig 2b). MnO polypods exposed (100), (001), and (010) planes on their branches (Fig 2c). These results further support the growth mechanism as aforementioned. The free OA ligands have a favorable interaction with (111) planes with a slightly larger surface energy, resulting in the anisotropic growth of MnO nanocrystals. For MnO octahedral NPs, the corresponding SAED pattern (Fig 2e) can be indexed as the <110>

zone axis of the MnO *fcc* structure. Only (111) planes are exposed for octahedral NPs. This is similar to previously reported FeO and CuO octahedral NPs.[8]
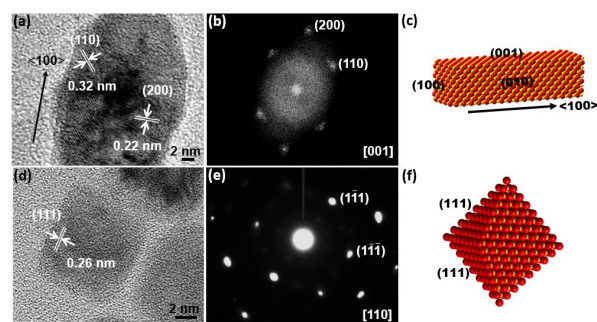
Fig 2. (a,b) The high-resolution TEM image of a single rod of MnO polypods (a) and the corresponded SAED pattern (b). (c) The schematic illustration indicating the growth direction and exposed planes of MnO nanorods on MnO polypods. (d,e) The high-resolution TEM image of a single MnO octahedral NP (d) and the corresponding SAED pattern (e). (f) The schematic illustration indicating the growth direction of MnO octahedral NPs. O is red and Mn is yellow.

In addition to pure MnO nanocrystals, other transition metal cations, *e.g.* Co^{2+}, can be doped into the complex nanostructure of MnO by mixing metal oleate precursors. TEM images of Co-doped MnO nanoflowers with Co/Mn molar ratios of 5% and 10% were given in Fig S9. The 3-D topological architectures of nanoflowers did not significantly change with the doping amount of Co cations. With 5% of Co, the diameter of Mn-Co nanoflowers was 95.8 ± 14.2 nm (Figs S9c) and nanorods appeared to pack more densely on the surface; while further increase of the Co/Mn molar ratio to 10% would lead to the increase of their average size to 186.2 ± 18.1 nm. Energy-dispersive X-ray elemental mapping confirmed the uniform distribution of Mn and Co elements in nanoflowers (Figs S9d~g). No change in the MnO crystalline structures was observed from XRD after doping (Fig S12).
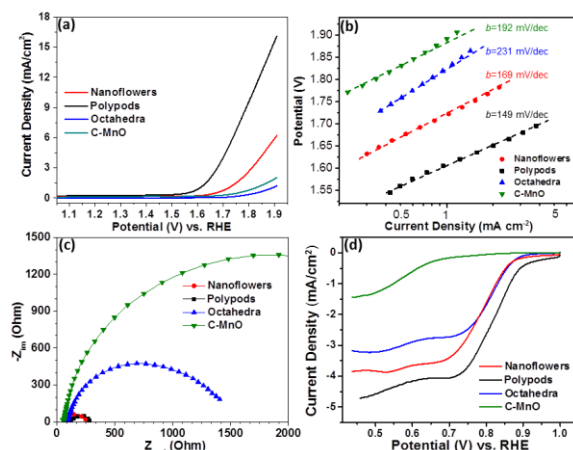
Fig 3. (a) Linear sweep voltammetry (LSV) curves of MnO nanocatalysts for electrochemical OERs at a scan rate of 5 mV s^{-1} in 0.1 M of KOH. C-MnO is commercialized MnO. (b) The corresponded Tafel plots of MnO nanocatalysts in (a). (c) The Nyquist plots obtained from the electrochemical impedance spectroscopy measurements at 1.76 V *vs.* RHE and a frequency range of 0.1 to 10^5 Hz. (d) Linear sweep voltammetry (LSV) curves for ORRs in 0.1 M of KOH solution.

MnO nanocrystals were further evaluated as bifunctional catalysts for the OER and ORR using rotating-disk electrode techniques. Fig 3a presents the typical linear sweep voltammograms

(LSVs) of MnO nanocrystals for OERs in KOH solution (0.1 M) with a sweep rate of 5 mV s^{-1}. MnO polypods with exposed (100) planes showed a superior activity with an overpotential (η) of 0.58 V at a current density (j) of 10 mA cm^{-2}, much lower than that of other MnO nanocrystals. At η=0.35 V, the mass activity for MnO polypods catalyst was found to be 17.75 A g^{-1}. The turnover frequency (TOF) of MnO polypods reached 4.19×10^{-4} s^{-1} (see Table S1), comparable with the reported best values of MnO$_x$ polymorphs.[5a,f,8a,9] MnO octahedra with (111) dominated surface exhibited a much lower activity and current densities, nearly overlapped with that of commercial MnO catalysts. MnO nanoflowers with multi-exposed planes displayed a moderate catalytic activity with a TOF of 1.32×10^{-4} s^{-1}. Tafel plots derived from LSV curves are given in Fig 3b. Tafel slopes of MnO polypods and nanoflowers are 149 and 169 mV/dec, respectively. The lower Tafel slopes indicate that the OER of polypods and nanoflowers is kinetically more favorable compared to that of octahedra. Fig 3c shows the Nyquist plot of the electrochemical impedance spectra (EIS) of MnO nanocrystals. The charge-transfer resistance value is inversely proportional to the electron transfer rate. MnO polypods and nanoflowers have R_{ct} of 256 and 275 Ω, respectively, lower than that of MnO octahedra and commercial MnO. This result is in good agreement with their OER activities.

ORR activity of MnO nanocrystals was also examined by cyclic voltammetry (CV) in 0.1 M of KOH solution. In argon-saturated solution, the voltammogram without an obvious peak was observed (Fig S14); while, a well-defined cathodic oxygen reduction peak with a high current density appeared when the electrolyte was saturated with O$_2$, indicating MnO nanocrystals are electrocatalytically active for the ORR. The ORR catalytic results of MnO nanocrystals are given in Fig 3d. MnO polypods, again, displayed a superior activity with a half-wave potential of 0.77 V, only 80 mV lower than that of Pt/C catalysts.[5f] The diffusion-limiting current of MnO polypods reaches ~5.0 mA cm^{-2}, higher than MnO nanoflowers with 3.8 mA cm^{-2} and octahedra with 3.1 mA cm^{-2}, indicating that the preferentially exposed (100) planes indeed improved the ORR activity as well. As compared to other reported MnO$_x$ catalysts for ORRs, e.g. MnO$_x$ film reported by Gorlin et al. with a potential of 0.73 V[5f] and α-MnO$_2$ reported by Meng et al. with a potential of 0.76 V at J=-3 mA cm^{-2},[5a] MnO polypods have some of the lowest overpotentials for the ORR. The stability of MnO ploypods for the ORR was also studied by current-time (i-t) chronoamperometric response at a potential of 0.66 V (vs. RHE) (Figure S17). MnO ploypods maintained 80% of its original activity after an hour. Furthermore, the overall oxygen electrode activity (ΔE=E_{OER}-E_{ORR}) is as low as 1.02 V, smaller than that of Ir/C and Pt/C,[3,4,5f] suggesting MnO polypods as a superior bifunctional electrocatalyst for OER/ORR.

For MnO (100) and (111) crystal planes, the (100) planes with mixed Mn^{2+} and O^{2-} ions have a lower surface energy; while, the (111) planes are polar surfaces consisting of alternating layers of Mn^{2+} and O^{2-} ions generating an electrostatic dipole field perpendicular to the surface. To gain further insight into the correlation between OER/ORR activities and the exposed crystal planes of the MnO nanocrystals, adsorption energies of O species, e.g. OH$^-$ and O$_2$ have been estimated for different MnO crystal planes (Table S2) using density functional theory. The adsorption of O species is known as a rate-determining step for ORRs/OERs.[10] In comparison with (111) planes, the MnO (100) planes are highly exothermic for OH$^-$ and O$_2$ adsorption. The large exothermic interaction may also be understood in terms of the unsaturated coordination on MnO (100) planes.

In summary, 3-D complex anisotropic MnO nanocrystals were demonstrated as superior bifunctional electrocatalysts. Their electrocatalytic activity for OERs/ORRs was strongly correlated with exposed lattice facets of MnO nanocrystals. The MnO (100) planes with higher adsorption energy of O species could largely promote the electrocatalytic activity for the OER and the ORR. Our results may illustrate a new paradigm for developing highly active and cost-effective electrocatalysts.

Acknowledgements

Notes and references

^{a} Department of Chemistry, ^{b} Department of Materials Science and Engineering and Institute of Materials Science, University of Connecticut, Storrs, CT 06269 USA.
E-mail: steven.suib@uconn.edu (SS); jie.he@uconn.edu (JH)

† Electronic Supplementary Information (ESI) available: Experimental details, characterization, computational details, and additional results for electrochemical studies. See DOI: 10.1039/b000000x/

(1) (a) Voiry, D.; Yamaguchi, H.; Li, J.; Silva, R.; Alves, D. C. B.; Fujita, T.; Chen, M.; Asefa, T.; Shenoy, V. B.; Eda, G.; Chhowalla, M. Nat. Mater. 2013, 12, 850. (b) Ji, X.; Lee, K. T.; Holden, R.; Zhang, L.; Zhang, J.; Botton, G. A.; Couillard, M.; Nazar, L. F. Nat. Chem. 2010, 2, 286. (c) Liang, Y.; Li, Y.; Wang, H.; Zhou, J.; Wang, J.; Regier, T.; Dai, H. Nat. Mater. 2011, 10, 780.
(2) (a) Bing, Y.; Liu, H.; Zhang, L.; Ghosh, D.; Zhang, J. Chem. Soc. Rev. 2010, 39, 2184. (b) Zhang, H.; Jin, M.; Xia, Y. Chem. Soc. Rev. 2012, 41, 8035. (c) Guo, S.; Zhang, S.; Sun, S. Angew. Chem. Int. Ed. 2013, 52, 8526. (d) Guo, S.; Zhang, X.; Zhu, W.; He, K.; Su, D.; Mendoza-Garcia, A.; Ho, S. F.; Lu, G.; Sun, S. J. Am. Chem. Soc. 2014, 136, 15026.
(3) (a) Koenigsmann, C.; Santulli, A. C.; Gong, K.; Vukmirovic, M. B.; Zhou, W.-p.; Sutter, E.; Wong, S. S.; Adzic, R. R. J. Am. Chem. Soc. 2011, 133, 9783. (b) Zhang, S.; Zhang, X.; Jiang, G.; Zhu, H.; Guo, S.; Su, D.; Lu, G.; Sun, S. J. Am. Chem. Soc. 2014, 136, 7734. (c) Strasser, P.; Koh, S.; Anniyev, T.; Greeley, J.; More, K.; Yu, C.; Liu, Z.; Kaya, S.; Nordlund, D.; Ogasawara, H.; Toney, M. F.; Nilsson, A. Nat. Chem. 2010, 2, 454.
(4) Reier, T.; Oezaslan, M.; Strasser, P. ACS Catal. 2012, 2, 1765.
(5) (a) Meng, Y.; Song, W.; Huang, H.; Ren, Z.; Chen, S.-Y.; Suib, S. L. J. Am. Chem. Soc. 2014, 136, 11452. (b) Indra, A.; Menezes, P. W.; Zaharieva, I.; Baktash, E.; Pfrommer, J.; Schwarze, M.; Dau, H.; Driess, M. Angew. Chem. Int. Ed. 2013, 52, 13206. (c) Najafpour, M. M.; Ehrenberg, T.; Wiechen, M.; Kurz, P. Angew. Chem. Int. Ed. 2010, 49, 2233. (d) Boppana, V. B. R.; Jiao, F. Chem. Commun. 2011, 47, 8973. (e) Iyer, A.; Del-Pilar, J.; King'ondu, C. K.; Kissel, E.; Garces, H. F.; Huang, H.; El-Sawy, A. M.; Dutta, P. K.; Suib, S. L. J. Phys. Chem. C 2012, 116, 6474. (f) Gorlin, Y.; Jaramillo, T. F. J. Am. Chem. Soc. 2010, 132, 13612. (g) Kuo, C. H.; Li, W.; Pahalagedara, L.; El-Sawy, A. M.; Kriz, D.; Genz, N.; Guild, C.; Ressler, T.; Suib, S. L.; He, J. Angew. Chem. Int. Ed. 2015, 54, 2345. (h) Huynh, M.; Bediako, D. K.; Nocera, D. G. J. Am. Chem. Soc. 2014, 136, 6002. (i) Jiao, F.; Frei, H. Chem. Commun. 2010, 46, 2920.
(6) Suib, S. L. Acc. Chem. Res. 2008, 41, 479.
(7) (a) Narayanaswamy, A.; Xu, H.; Pradhan, N.; Peng, X. Angew. Chem. Int. Ed. 2006, 45, 5361. (b) Ould-Ely, T.; Prieto-Centurion, D.; Kumar, A.; Guo, W.; Knowles, W. V.; Asokan, S.; Wong, M. S.; Rusakova, I.; Lüttge, A.; Whitmire, K. H. Chem. Mater. 2006, 18, 1821. (c) Zitoun, D.; Pinna, N.; Frolet, N.; Belin, C. J. Am. Chem. Soc. 2005, 127, 15034.
(8) (a) Kim, D.; Lee, N.; Park, M.; Kim, B. H.; An, K.; Hyeon, T. J. Am. Chem. Soc. 2008, 131, 454. (b) Cheon, J.; Kang, N.-J.; Lee, S.-M.; Lee, J.-H.; Yoon, J.-H.; Oh, S. J. J. Am. Chem. Soc. 2004, 126, 1950. (c) Liang, X.; Gao, L.; Yang, S.; Sun, J. Adv. Mater. 2009, 21, 2068.
(9) Zaharieva, I.; Chernev, P.; Risch, M.; Klingan, K.; Kohlhoff, M.; Fischer, A.; Dau, H. Energy Environ. Sci. 2012, 5, 7081.
(10)(a) Lima, F. H. B.; Calegaro, M. L.; Ticianelli, E. A. Electrochim. Acta 2007, 52, 3732. (b) Mao, L.; Zhang, D.; Sotomura, T.; Nakatsu, K.; Koshiba, N.; Ohsaka, T. Electrochim. Acta 2003, 48, 1015.

ARTICLE TYPE

Table of Content
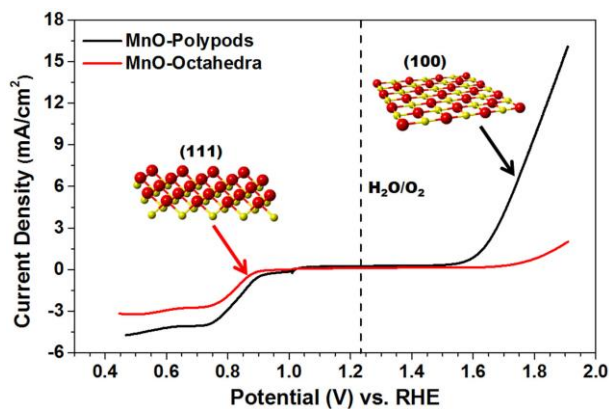
The MnO (100) facets with higher adsorption energy of O species can largely promote the electrocatalytic activity.

ChemComm Accepted Manuscript